Kinetic Programmed Resuspension - KPR Technique

J.G. Benito [a], R.O. Uñac [a], A.M. Vidales [a] and I. Ippolito [b]

(a) INFAP, CONICET, Departamento de Física, Facultad de Ciencias Físico Matemáticas y Naturales, Universidad Nacional de San Luis, Ejército de los Andes 950, D5700HHW, San Luis, Argentina.
(b) Grupo de Medios Porosos, Facultad de Ingeniería, Universidad de Buenos Aires, Paseo Colón 850, 1063, Buenos Aires, Argentina.

Abstract

In particle resuspension phenomena, experimental and simulation evidence demonstrate that, as the acceleration increases, higher air velocities are needed for particle re-entrainment, and the process requires less time to develop. In order to describe this problem and to shed light to its understanding, we present in this paper a new analysis named Kinetic Programmed Resuspension (KPR). This new insight into the kinetics of the resuspension process provides a technique for determining some resuspension experimental parameters. Thereby, using a simple Monte Carlo model, we are able to reproduce experimental data and, from these results, to analyze the main kinetic parameters involved, just by analogy with the process of thermal desorption of molecules from surfaces.

Keywords: Resuspension; Monte Carlo simulation; kinetic; air acceleration.

1. Introduction

The problem of resuspension of already deposited fine particles on a surface has been subject of special attention for researchers since many decades. This phenomenon is present in a wide range of fields, such as resuspension of airborne particles, re-entrainment of sediments, human health, filtration systems and food industry (Bowling, 1988). Besides, the problem of resuspension causes serious difficulties in mining production. Indeed, mining operations are notable in the amount of particulates generated and the extent of polluted areas and toxicity, when compared with other sources of dust and aerosol emissions (Csavina et al., 2012; Stovern et al., 2014). Furthermore, resuspension phenomenon is essential in the study of radioactive particles released to the environment during nuclear accidents (Reeks et al., 1988; Stempniewicz et al., 2008; Zhang et al., 2013).

However, many aspects of the problem still remain as an open question for researchers. Resuspension involves particles with different properties as well as a wide range of scales. One of the difficulties lies in the determination of the microscopic adhesion forces that result from the particles-surface interaction through a blend of mechanical stress, chemical bonds and physical attractions, where roughness plays an essential role. Other difficulties are the different flow conditions and the respective aerodynamic forces involved. Consequently, given the experimental complexity in their determination, a theoretical approach is required to model particle-surface interactions.
All these open issues, among others, make resuspension to remain the object of ongoing investigations.

There are many comprehensive reviews concerning resuspension models in the literature (Ziskind et al., 1995; Stempniewicz et al., 2008; Zhang, 2011; Henry and Minier, 2014a and 2014b).
Many models are based on a balance of forces that propose an instantaneous resuspension of particles when the removal forces are greater than the adhesion forces (Reeks et al., 1988). On the other hand, there are models allowing the movement of the particle on the surface before re-entrainment, usually including a balance of moments acting on it (Guingo and Minier, 2008; Henry et al., 2012; Fu et al., 2013; Henry and Minier, 2014b). As one can expect, the choice of a force balance or a moment balance approach is related to the assumed motion of particles: rolling, described by moment balance, while sliding and lifting are properly described by a force balance (Ibrahim et al., 2008).
The basis for the analogy of the resuspension phenomenon with the desorption of molecules is first presented in Reeks, Reed and Hall (1988). There, the authors assume that there are enough particles on the surface to form an ensemble of all the possible states for a single particle in a constant potential well. If the particle receives enough energy from the local turbulence to overcome the potential well, it will leave the surface (resuspend). The idea behind is deterministic in nature, given that the potential barrier has to be surpassed by the particle.
On the other hand, Wen and Kasper (1989) developed a kinetic model based on the analogy between the process of resuspension and the kinetics of the first order reaction that describes the molecules desorption from a heterogeneous surface. This kind of modeling opens the possibility to handle the resuspension phenomenon as a stochastic process.
Recently, we have proposed a model based on a Monte Carlo (MC) simulation that takes advantage of the phenomenological Arrhenius expression for the determination of the

resuspension rate (Benito et al., 2015 and 2016). We have shown that the Metropolis function (Binder and Heermann, 1992), used as the transition probability between configuration states, is able to describe the principal characteristics of the particle resuspension for the case of a monolayer of particles deposited on a flat surface and subjected to air flow. We have proved that a Monte Carlo model based on a moment balance reproduces quite well experimental results (Benito et al., 2016). Moreover, the rolling mechanism shows to be crucial to explain the detachment process of the particles from the surface. This is in agreement with the conclusions reached by Reeks and Hall (2001) and Ibrahim et al. (2003) who established that although particles can slide or directly be pulled-off, these mechanisms are not significant compared to the rolling one.

Typical resuspension experiments are performed inside a wind tunnel where micro-particles are subjected to an air flow. Even though a possible experiment could be performed at constant air flow velocity, a transient velocity condition is experimentally inevitable. Thus, wind acceleration is one experimental parameter that controls resuspension phenomena (Matsusaka and Masuda, 1996; Ibrahim et al., 2006; Soltani and Ahmadi, 2006).

Ibrahim et al. (2006) have analyzed the effects of the temporal flow acceleration experimentally. They used 70 μm stainless microspheres deposited on glass substrate and subjected to temporal acceleration ranging from 0.01 to 2 m/s^2. They found that for relatively slow flow acceleration (0.3 m/s^2 or less) particle detachment was independent of the acceleration within the experimental uncertainty range. For higher accelerations, the threshold velocity U_{th} (required to detach one half of the particles) increased with acceleration. They showed that temporal flow acceleration postponed the transition to turbulence, reducing the wall shear stress and burst-sweep events and, thereby suppressing detachment.

In this study, we will focus on a detailed analysis of the influence of air flow acceleration using our MC numerical model developed earlier (Benito et al., 2015). A summary of the numerical model is presented in section 2, while the results obtained through the Monte Carlo model for different velocity rates are analyzed in section 3. In order to understand the kinetics of the resuspension phenomenon, section 4 is dedicated to the development of a novel methodology (Kinetic Programmed Resuspension) from which a potential tool for the determination of resuspension experimental parameters is derived. A detailed analysis of the potentiality of this Kinetic Programmed Resuspension technique is

presented in section 5, in which experimental data is used for examining its performance. Finally, conclusions are presented in Section 6.

2. Resuspension Model

The model used for the resuspension of particles from a surface is based on a Monte Carlo method (MC) (Benito et al., 2015, 2016). Taking into account the similitude between the resuspension phenomenon and a desorption process from a heterogeneous surface; we assume that the rate equation follows the Arrhenius law (Hughes, 1971).

MC methods have been used for decades as versatile tools to describe molecular processes on surfaces (Binder and Heermann, 1992) and different extensions of this method have been proposed in order to take into account the kinetic mechanisms governing the resuspension of particles from a surface (Reeks, Reed and Hall, 1988; Wen and Kasper, 1989). In other words, and citing former works (Fichthorn and Weinberg, 1991), Monte Carlo methods can be utilized to simulate effectively a Poisson process if three criteria are met, this means, a "dynamical hierarchy" of transition probabilities satisfying the detailed-balance criterion; appropriate time increments; and the achievement of the effective independence of various events comprising the system. In this way, both static and dynamic properties of model Hamiltonian systems may be obtained and interpreted consistently.

A detailed description of the MC method based on the Metropolis function can be found in Benito et al. (2015, 2016). Briefly, we recall that assuming a N-particle system and considering only one possible type of transition, i.e., a deposited particle can resuspend to the gas stream, the probability *P(t)dt* of the system to perform a transition during the interval (*t; t+dt*) is given by a Poisson process (Sales et al., 1996)

$$P(t)dt = Re^{-Rdt} \tag{1}$$

where $R = \sum_{i=0}^{N} r_i$ is the total transition rate for the whole system of N particles and r_i is the resuspension transition rate for a single particle. The variable t, which is distributed following $P(t)dt$, is replaced by a random number ξ, uniformly distributed in the interval (0; 1) (Sales et al., 1996)

$$\Delta t = -\frac{\ln(\xi)}{R} \tag{2}$$

Equation 2 gives the actual time in which the system performs a transition.

Thus, the total transition rate R (which is known in the simulation) along with Eq. 2, determine the relationship between the "virtual" MC time and the "actual" time of the system. Besides, when the transitions are carried out in equal time intervals, Δt, the actual elapsed time after N_s MC steps is simply $t = N_s \Delta t$ (also referred as Kinetic Monte Carlo simulation).

For all the simulations we consider an idealized lattice structure of a monolayer deposit of N_0 =10000 mono-sized particles with radius R_p. The distance between particles is not relevant since they do not interact with each other and collision effects are not considered. We take into account the resuspension of the particles deposited on the flat surface as a process activated by the turbulent air flow and, in our model, particles are not allowed to be re-deposited or re-located.

In previous works (Benito et al., 2015 and 2016) we have described two different model versions based on the possibility of expressing the transition rate for the Arrhenius type process in two different ways: one related to the balance of forces acting on the particle and the other related to the balance of the moments acting on it.

It should be noted that these MC versions of the model have been contrasted with previous experimental results (Reeks and Hall, 2001; Ibrahim et al., 2003). It was concluded that the best approximation to these experimental results was achieved with the moment balance model. This fact emphasized that the dominant take-off mechanism (for later resuspension) was rolling, which was also in agreement with the conclusion of others authors (Ibrahim et al., 2003; Reeks and Hall, 2001; Goldasteh et al., 2013; Guingo and Minier, 2008; Fu et al., 2013).

Indeed, a previous work (Reeks and Hall, 2001) revised the so called RRH model (Reeks, Reed and Hall, 1988) to account for drag as well as lift effects in the rocking of the particle around the asperities in the contact. The basic formula for the resuspension rate is basically the same as in the original RRH model, except that the potential energy now depends upon the torque acting on the particle (including therefore the influence of drag as well as lift) and the moment of inertia of the particle about the pivot. In this sense, here we recover this idea to include the moment balance in the calculation of the transition rate for the resuspension phenomena.

Taking into account the moment balance model, we assume that each particle belonging to the defined arrangement is attached to the surface (substrate) by an adhesion force, and to be exposed to air flow that exerts aerodynamic forces and moments on it. Figure 1 shows the force diagram for a particle of radius R_p. This diagram includes five forces: the gravitational force, F_g (mg), the adhesion force, F_a, the lift force, F_L, in the upward

vertical direction, the drag force, F_d, in the forward horizontal direction. Both F_L and F_d are caused by the aerodynamic effects.

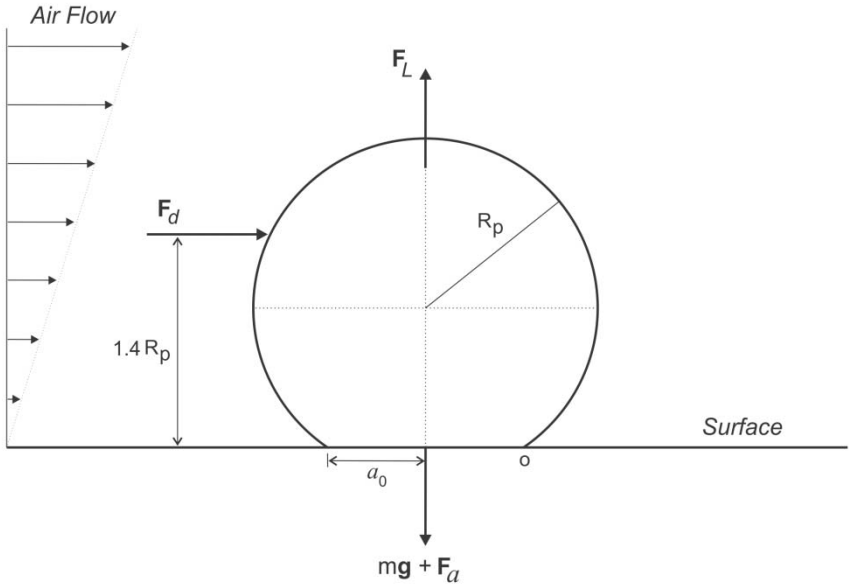

Figure 1:Particle Force diagram

Rolling detachment mechanism would take place only if the moments of the aerodynamic forces exceed the moments of the adhesive and gravity forces (Ibrahim et al., 2003):

$$(1.4R_p)F_d + a_0F_L > a_0(F_a + F_g) \tag{3}$$

The contact radius a_0 is evaluated assuming the JKR theory for a smooth surface

$$a_0 = \left(\frac{6\pi\gamma R_p^2}{4K}\right)^{1/3} \tag{4}$$

Where γ is the surface energy of adhesion and K the composite Young's modulus

$$K = \frac{4}{3}\left[\frac{(1-\nu_1^2)}{E_1} + \frac{(1-\nu_2^2)}{E_2}\right]^{-1} \tag{5}$$

with E_1 and E_2 the values of Young's modulus and ν_1 and ν_2 the values of Poisson's ratios for the particle and the surface, respectively.

Taking into account that rolling is the only motion responsible for the resuspension, we define the transition rate r_{roll} from the moment balance condition:

$$r_{roll} = k\exp\left(-\frac{\left[a_0(F_a + F_g) - (1.4R_pF_d + a_0F_L)\right]}{(1.4R_pF_d + a_0F_L)}\right) \tag{6}$$

where k is a frequency factor that can be interpreted as the maximum burst frequency in the removal process.

The adhesion force, F_a, used in this model is sampled from a lognormal distribution (Bohme et al., 1962; Reeks et al., 1988; Matsusaka et al., 1991; Taheri and Bragg, 1992; Reeks and Hall, 2001; Salazar-Banda et al., 2007; Zhang et al., 2013). Its form is given by

$$A(F_a) = \frac{1}{\sqrt{2\pi}F_a \ln \sigma_a} \exp\left(-\frac{1}{2}\left(\frac{\ln \frac{F_a}{\mu_a}}{\ln \sigma_a}\right)^2\right) \tag{7}$$

Where μ_a and σ_a are the mean and the dispersion, respectively. In order to account for the roughness effects, we consider that the mean adhesion force is a certain percentage of the force value corresponding to a smooth contact (F_{JKR}) (Johnson et al., 1971; Reeks and Hall, 2001; Ibrahim et al., 2003, 2008). Thus, the mean μ_a can be written as

$$\mu_a = \frac{F_{JKR}}{f_r} \tag{8}$$

The reduction factor f_r takes into account the contact geometry in a real surface which is characterized by a wide distribution of surface roughness. As already known, this will produce, at the same time, a reduction of the mean value and a spread in the force of adhesion compared with a perfectly smooth contact (Reeks and Hall, 2001). Both, f_r and σ_a would remain as model parameters. It is worth noting that the value of F_a assigned to each particle in the initial arrangement remains the same throughout the simulation. This is related to the fact that no rearrangements or particle motion are present on the surface. On the other hand, lift forces are assumed to obey a Gaussian distribution as (Reeks and Hall, 2001)

$$B(F_L) = \frac{1}{\sqrt{2\pi}\sigma_L} \exp\left(-\frac{1}{2}\left(\frac{F_L - \mu_L}{\sigma_L}\right)^2\right) \tag{9}$$

where μ_L and σ_L are the mean and the dispersion, respectively. For the mean value of the lift force distribution we follow the assumptions made by other authors (Mollinger and Nieustadt, 1996; Ibrahim et al., 2003; 2008)

$$\mu_L = (56.9 \pm 1.1)\rho_f \nu^2 \left(\frac{R_p u^*}{\nu}\right)^{(1.87 \pm 0.04)} \tag{10}$$

Here ρ_f is the air density, u^* the friction velocity and ν the air kinematic viscosity. We also set σ_L = 0.33μ_L, which reasonably represents the range of experimental values reported in the literature (Popovitch and Hummel, 1967; Friess and Yadigaroglu, 2001; Zhang et. al, 2013).

Finally, the drag forces are assumed to obey a Gaussian distribution given by a similar expression as Eq. 9 (Reeks and Hall, 2001). For this force distribution μ_d and σ_d would be the mean and the dispersion, respectively. The mean value of the drag force can be taken following the assumptions of other authors as: (Reeks et al. 2001; Friess and Yadigaroglu, 2001; Benito et al. 2014; 2016)

$$\mu_d = c_d \rho_f u^{*2} R_p^2 \tag{11}$$

Where c_d is a constant (typically between 20 and 32). We also set here σ_d = 0.33μ_d.

As a consequence of the time changes in the friction velocity u^*, the distributions of aerodynamic forces change.

A detailed step routine for the MC algorithm can be found in Benito et al. (2014; 2016).

3. Results for resuspension with accelerated air flows

In order to analyze the influence of the air flow acceleration α applied to the particles, we perform MC simulations using stainless steel spheres of radius 35 μm deposited on a glass surface. This particle-surface system has already been chosen in a previous work (Benito et al., 2016) to compare the MC model performance with other author's experimental data (Ibrahim et al., 2003). Table 1 summarizes all the system constants and simulation parameters selected.

Table 1: Simulation constants and particle-surface parameters.

JKR Adhesion force (N)	$1.61R_p$
Reduction Factor f_r	100 and 52
Adhesion dispersion σ_a	1.0

Surface energy γ (J/m^2)	0.15
Surface Young's modulus E_1 (GPa)	80.1
Surface Poisson's ratio ν_1	0.27
Particle Young's modulus E_2 (GPa)	215
Particle Poisson's ratio ν_2	0.28
Particle Density ρ (Kgm^{-3})	8000
Air Density ρ_f (Kgm^{-3})	1.2
Air kinetic viscosity ν (m^2/s)	1.45E-5
Drag force constant c_d	32.0
Frequency k (1/s)	1.0

As mentioned before, we are interested in analyzing the influence of the velocity rate on the resuspension kinetic. Thus, for the air flow conditions we considered that the free-stream velocity increases linearly with time, starting from 0, and with a constant acceleration α during each simulation run. In order to link the free-stream velocity U and the friction velocity u^*, we assume the linear relationship measured by Ibrahim et al. (2003), i.e., $u^* = 0.0375U + 0.0387$.

Following the MC algorithm, we record the particle fraction detached from the surface as a function of the friction velocity u^*.

Figure 2 shows the results of the resuspended particles as a function of u^* using three different accelerations for the air flow (which are within the typical experimental range used by Ibrahim et al. (2006)). As it can be seen, in all the cases particle detachment does not occur at a single air velocity but a velocity range exists in which the resuspension of all the particles on surface is reached. Thereby, our MC model is able to reflect the stochastic nature of the process which can be associated to the presence of burst in the air flow, dispersion of roughness scales, adhesion forces and size of the particles, among others.

Taking into account that resuspension occurs in a range of velocities, a threshold velocity u_{th}^* can be defined as the friction velocity at which the detachment fraction equals 0.50.

As it can be seen in Figure 2, increasing the wind acceleration α induces a shift of the curves to the right. This behavior can be noticed from the corresponding values of the threshold velocity while increasing α: 0.15, 0.21 and 0.27 m/s. For higher accelerations,

the threshold velocity obtained is also higher. This fact also indicates that in order to resuspend all the particles from the surface a wider range of velocities is needed as the acceleration increases.

The MC results presented in Figure 2 qualitatively agree with experimental ones, i.e., the mentioned trend of the MC curves was also observed in experiments performed by Ibrahim et al. (2006). It is important to notice that, in this section, we do not aim to reproduce with our model these experimental results, but rather to reflect the effect of the acceleration α in the typical curves.

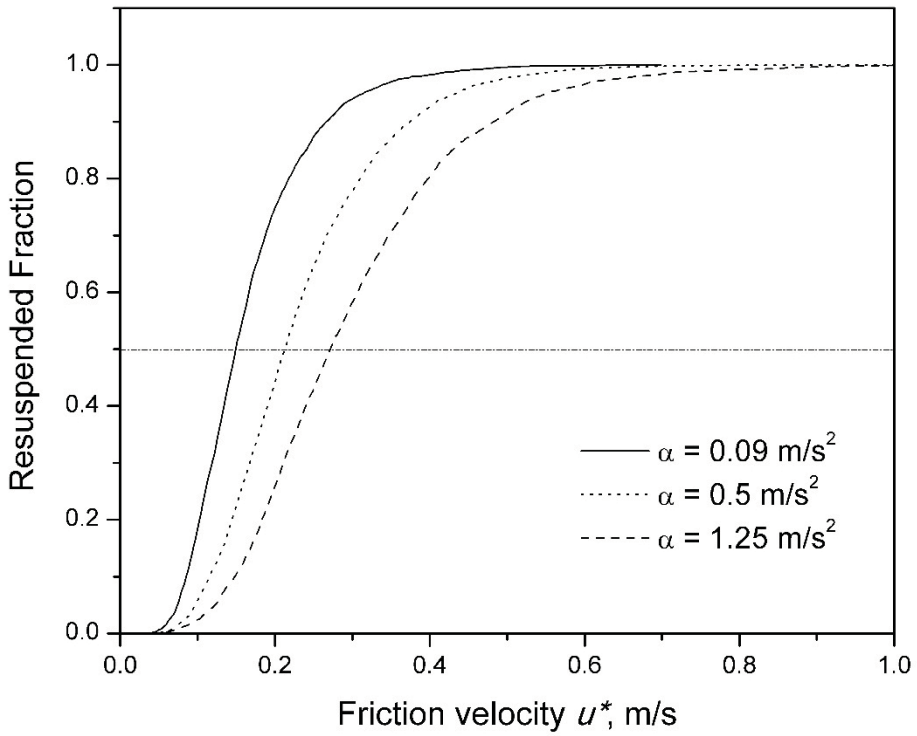

Figure 2: MC model results of Resuspended Fraction vs. Friction velocity u^* for three different accelerations. Dash-dotted horizontal line corresponds to a resuspended fraction of 0.5, from which the threshold velocity u_{th}^* was evaluated.

It is also worthy to mention that, even though we have shown results for three different α values, we have performed simulations using 0.09, 0.18, 0.35, 0.5, 0.75, 1.25 and 1.5 m/s^2 and, results for all of them are in agreement with the described behavior.

On the other hand, the MC results also allow us to analyze the evolution of the fraction of resuspended particles with time. Figure 3 shows three time curves corresponding to the acceleration cases presented in Figure 2. It can be noticed that despite of the need of a wider velocity range when increasing α, the time required for total particle

resuspension is lower as the acceleration increases; therefore, the resuspension process is faster.

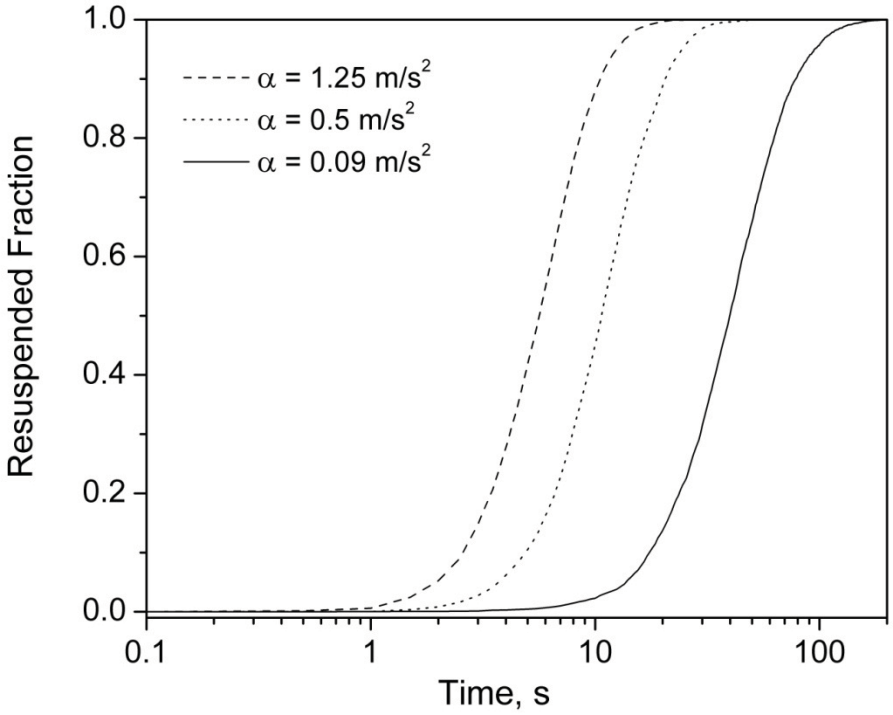

Figure 3: MC model results for Resuspended Fraction vs. Time corresponding to three different accelerations.

4. Kinetic Programmed Resuspension (KPR)

Results obtained up to now indicate that increasing the air flow acceleration leads to a change in resuspension phenomena. This change is related to the reduction of the wall shear stress and burst-sweep events in the near-wall region, as proved by Ibrahim et al. (2006). Nevertheless, there is a lack of information related to the kinetic of the particle flow as the acceleration increases. This is, the effect of acceleration induces both, a shift (or a delay) from a velocity point of view, and a reduction of the required time for the whole particle resuspension process. Thus, one could ask: How these two facts are related? In which way the kinetic of the resuspension process is affected by the velocity rate?

In order to answer these questions we have developed the KPR technique (Kinetic Programmed Resuspension) based on the analogy with the Temperature Programmed Desorption (TPD) technique (Spinicci, 1996; Wang, 1982; Falconer and Schwarz, 2007;

Redhead, 1962). This method is widely used for determining the activation energy, the rate constant and the order of the reaction during the desorption of molecules from surfaces. In particular, the activation energy of desorption for first-order reactions is estimated from the temperature at which the desorption rate is a maximum. It is important to note that this analogy is not straightforward, i.e., the TPD technique analyzes the chemical kinetic in molecular desorption processes activated by temperature while the KPR technique would be devoted to study the mechanical kinetic present in the resuspension phenomenon activated by the effect of aerodynamic forces due to the air velocity.

It can be noticed that in the transition rate r_{roll}, defined in Eq. 6, the moments exerted by the lift and gravitational forces are negligible. Indeed, if one compares the mean lift and drag forces values at a given velocity (Eqs. 10 and 11 respectively), it could be found that the order of magnitude is the same and, in fact, lift forces are slightly greater than the drag ones. Despite this, the differences in the corresponding lever arms (larger for the drag force) leads to a scheme where the effects of the drag force moment are dominant.

Taking into account these simplifications, the resuspension rate can be expressed as:

$$-\frac{dN}{dt} = kexp\left[-\frac{(M_a - M_d)}{M_d}\right]N = -keNexp\left(-\frac{M_a}{M_d}\right) \quad (12)$$

where we have simplified the exponent and, consequently, a factor number e appears in the equation. The moments of adhesion and drag forces are defined as $M_a = \mu_a a_0 = \frac{F_{JKR}}{fr} a_0 = \frac{1.61\, R_p}{fr} a_0$ and $M_d = 1.4 R_p \mu_d = 1.4 R_p c_d \rho_f R_p^2 u^{*2} = 1.4 c_d \rho_f R_p^3 u^{*2}$, respectively.

Thus, the resuspension rate or, in other words, the particle flux can be re-written as:

$$\frac{dN}{dt} = -keNexp\left(-A\frac{1}{u^{*2}}\right) \quad (13)$$

with $A = \frac{1.61 a_0}{1.4\, R_p^2 c_d \rho_f fr}$. This constant includes all the kinetic information related to the particle-surface system and air fluid parameters.

Given that we have analyzed particle resuspension for the case of a linear increase of the free stream velocity, i.e., $U = U_0 + \alpha t$ and that, in our simulations, $u^* = 0.0375U + 0.0387$, the particle flux can be expressed as:

$$\frac{dN}{dt} = \frac{dN}{du^*}\frac{du^*}{dU}\frac{dU}{dt} = 0.0375\alpha\frac{dN}{du^*} \tag{14}$$

Therefore, substituting Eq. 14 into 13 we get

$$-\frac{dN}{du^*} = \frac{ke}{0.0375\alpha}Nexp\left(-A\frac{1}{u^{*2}}\right) \tag{15}$$

Following the steps established in the TPD method (Redhead, 1962) the KPR technique would require obtaining the maximum friction velocity u^*_{max}, i.e., the friction velocity at which the particle flux reaches a maximum value. This can be obtained analytically from:

$$\left.\frac{d^2N}{du^{*2}}\right|_{u^*_{max}} = 0 = \frac{dN}{du^*} + N\frac{2A}{u^{*3}} \tag{16}$$

Thus, Eq. 16 states the condition to obtain the friction velocity required to obtain the maximum number of resuspended particles N. Using the last two equations, this condition can be written as:

$$\ln\left(u^{*3}_{max}\right) - ln\left(\frac{2A\alpha 0.0375}{ke}\right) - A\frac{1}{u^{*2}_{max}} = 0 \tag{17}$$

Therefore, starting from the expression for the resuspension rate, we achieve to a condition which enables us to estimate the velocity for the maximum resuspension rate, providing a more suitable characterization for the kinetic of the resuspension process. As it can be noted, this transcendental equation relates the friction velocity u^*_{max} with the air flow acceleration and the constant *A* defined above.

To better understand the information that the KPR technique is able to predict and, in order to illustrate the methodology, we have applied the KPR to our MC simulation results. Taking into account the particle resuspended fraction as a function of the velocity shown in Figure 2, the first step is to calculate, by deriving the curves, the flux of particles as a function of the friction velocity and for each acceleration value. These results are shown in Figure 4. As it can be seen, the particle flux is higher as the acceleration α is increased. This behavior agrees with the expectation of a faster particle resuspension for a higher acceleration value. On the other hand, results also indicate that there is an air velocity at which the resuspension process presents a maximum flow rate. The position or location of the maximum particle flux presents a shift to higher velocities as

the acceleration increases. For the cases shown in Figure 4, maximum flow rates are obtained for 0.14, 0.17 and 0.20 m/s, respectively.

It is worthy to mention that even though the velocities obtained for the maximum flow rates (u^*_{max}) are very close to the threshold velocity u^*_{th}, the maximum flow rate is achieved at a value which is always slightly lower than the threshold velocity related to the half resuspension fraction.

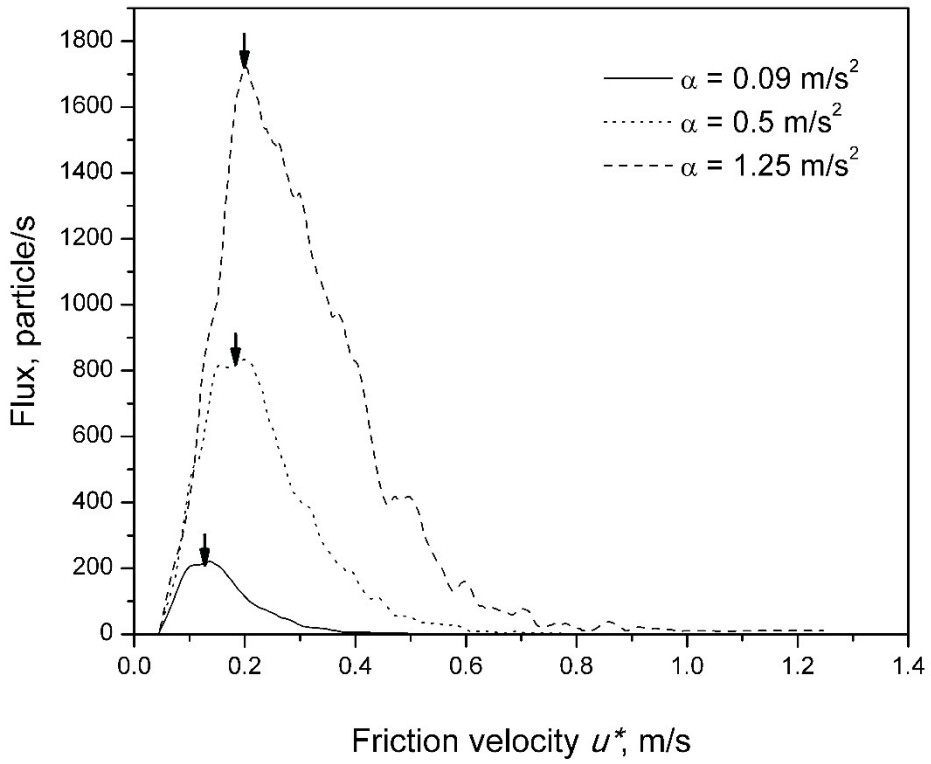

Figure 4: Particle Flux vs. Friction velocity u^* using our MC model, for three different accelerations. Vertical arrows indicate maximum's locations.

To continue the analysis, we compute the location of the maximum flow rate for all the simulation cases performed with different acceleration values (0.09, 0.18, 0.35, 0.5, 0.75, 1.25 and 1.5 m/s^2). These results along with the analytical prediction of the KPR technique are presented in Figure 5. In this figure, dots represent the values of u^*_{max} obtained by locating the maximum particle flux on the plots of flux vs. friction velocity, and the solid line represents the theoretical curve obtained from the transcendental Eq. 17. It is worth to mention that for the evaluation of this analytical curve, we have

calculated the constant $A = \frac{1.61 a_0}{1.4\, R_p^2\, c_d \rho_f f r}$ using the simulation parameters listed in Table 1 and with f_r equals to 100.

As it can be seen in Figure 5, the maximum velocities u_{max}^* increase with the acceleration α, following the KPR prediction (Eq. 17). Thus, the relationship between the acceleration and the maximum particle flow rate follows a non-trivial dependence. Besides, it can be observed that the increases of u_{max}^* becomes slighter as the acceleration increases.

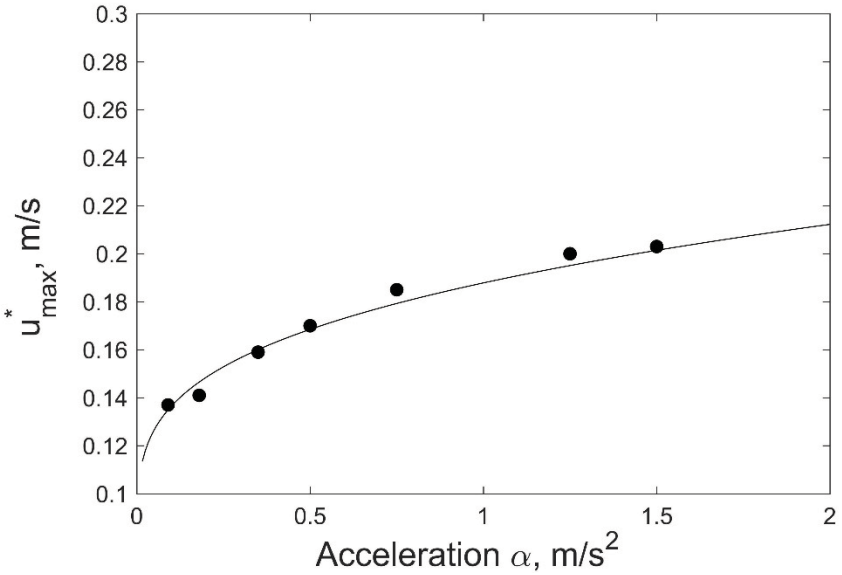

Figure 5: Dependence of the u_{max}^* as a function of the air flow acceleration. Symbols represent the maximum velocities obtained through our MC curves for different accelerations. Solid line represent the KPR prediction from Eq. 17.

One step forward into a better comprehension of the KPR technique and its advantages could be derived from the analysis of the capability of this method to predict particle-surface system characteristics. A possible application of the KPR links to the determination of unknown variables through the repetition of resuspension experiments in a wind tunnel with a suitable control of the velocity rate. If one could compute numerous repetitions of experiments for different values of air acceleration, the KPR method would allow obtaining the constant *A* in Eq. 17 and, through it, one of the system parameters.

Equation 17 can be alternatively expressed as:

$$\ln\left(\frac{\alpha}{u_{max}^{*\,3}}\right) = ln\left(\frac{ke}{2\ 0.0375A}\right) - A\frac{1}{u_{max}^{*\,2}} \qquad (18)$$

This indicates that plotting the $\ln\left(\frac{\alpha}{u_{max}^{*\,3}}\right)$ as a function of $\frac{1}{u_{max}^{*\,2}}$, one could expect a linear trend, with a slope equal to $-A$ and an intercept of value $ln\left(\frac{ke}{2\ 0.0375A}\right)$. This can be observed in Figure 6. Following the procedure above, we plot the natural logarithm of $\frac{\alpha}{u_{max}^{*\,3}}$ as a function of $\frac{1}{u_{max}^{*\,2}}$ for each MC simulation result with a different acceleration value. As it can be noticed, a linear trend behavior is obtained. Comparing the value of the constant *A* obtained through the slope of this linear trend (0.046 m^2/s^2) with the calculated one from the input parameters used in the MC simulations (0.053 m^2/s^2), the estimation is quite good, within an error less than 15%.

In this way, the repetition in the acquisition of the velocity at which the particle rate is maximum at a given air flow acceleration facilitates the estimation of the constant *A* or of one of the unknown parameters included in it.

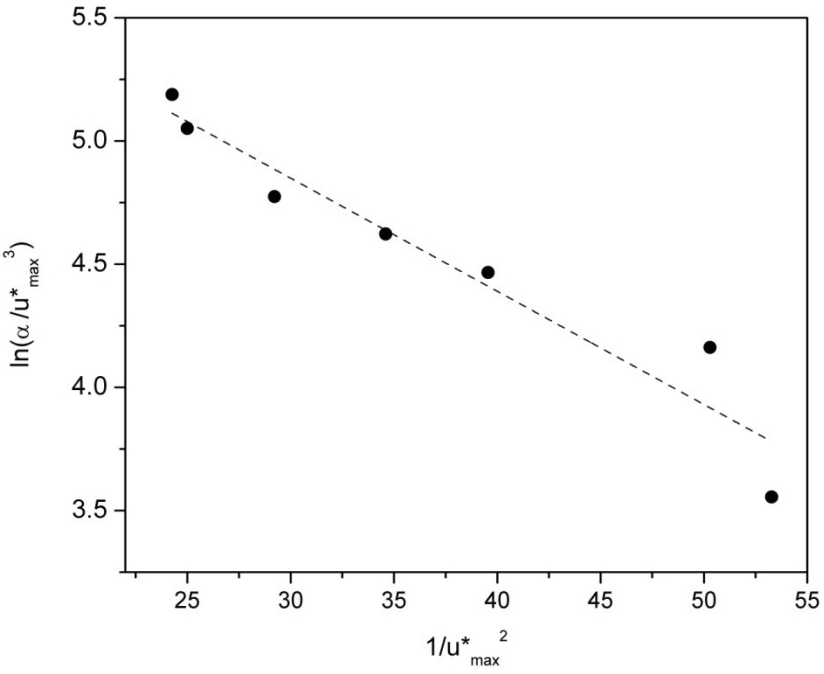

Figure 6: Illustration of the KPR application for the estimation of the unknown particle-surface constant *A*.

Finally, in order to complement the results for the resuspension time presented in the section before, Figure 7 shows the Particle Flux (obtained through MC model) as a function of time for different accelerations. Here again, as in Figure 4, these curves present a maximum which is higher as the acceleration increases. Nevertheless, the location of these maximum values shift to the right as the acceleration decreases. This

behavior reinforces the fact that, when increasing the acceleration, one could expected both, a greater particle flux and a faster process.

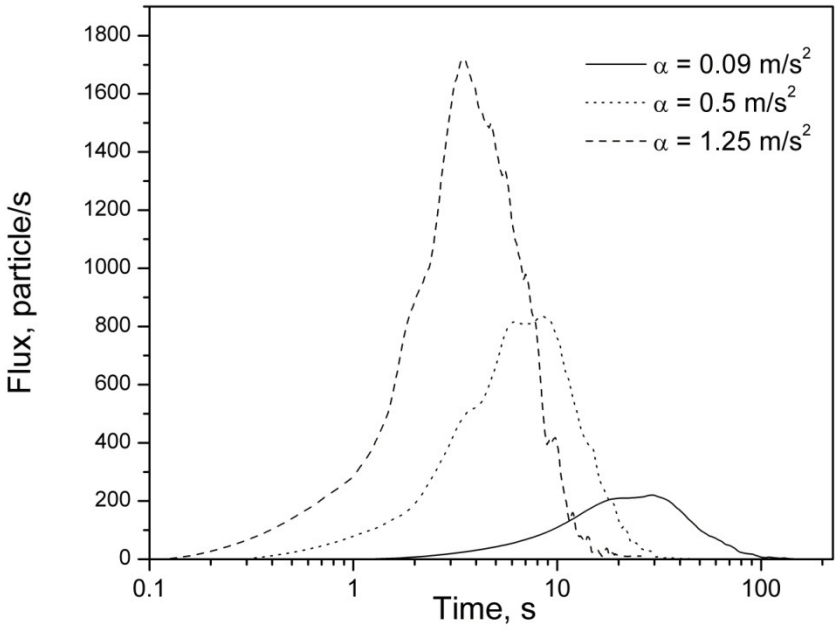

Figure 7: Particle Flux vs. Time for three different accelerations obtained from our MC model results.

5. KPR- technique capability: Discussion

In order to try out the capability of the KPR technique proposed here, we have applied its basic steps in the experimental dataset performed by Ibrahim et al. (2006). As mentioned in the Introduction, these authors present a study of the influence of the flow acceleration on the resuspended fraction of stainless steel particles (70 μm diameter). The results for the resuspended fraction as a function of the free-stream velocity U using different accelerations reflect the fact that the resuspension does not occur at a single velocity, but rather inside a velocity range. Thereby, for each acceleration tested in their experiments, the curves obtained follow a pronounced sigmoidal behavior.

To avoid the noise that a discrete function with few points could introduce to its derivative, we first fit each experimental curve (Fig. 5 from Ibrahim et al., (2006)) with a sigmoid function, obtaining an analytical expression of the resuspended fraction as a function of the velocity U for each acceleration ramp.

Then, as the KPR technique indicates, we calculate the flux as a function of the velocity by deriving these analytical curves. The results for three different accelerations (0.09, 0.27, 0.97 m/s^2) are presented in Figure 8.

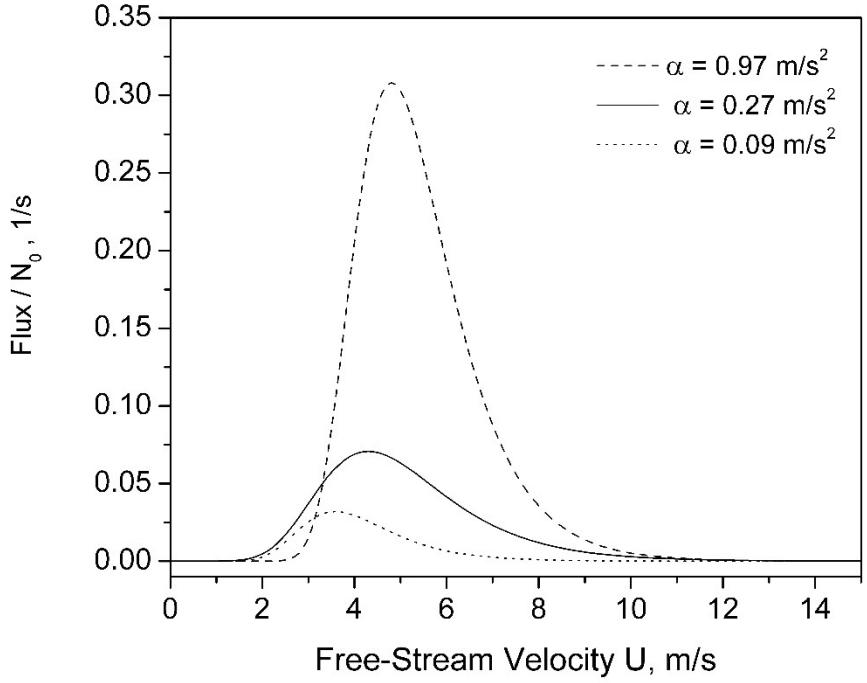

Figure 8: Particle Flux vs. Free-Stream Velocity U for three different accelerations, obtained from the experimental data analysis of Ibrahim et al. (2006).Vertical axis represents the Flux divided the initial amount of particles.

As it can be seen, the experimental particle flux is in fact higher as the acceleration α increases, like was predicted by the KPR formulation in section 4. In this way, experimental results show that the kinetic process is faster as the acceleration increases.

Besides, the analysis of the experimental data clearly shows the existence of a maximum flow rate. Even more, the location of the maximum particle flux indeed shifts to higher velocities as the acceleration increases.

The maximum particle flux rates in these experiments are located at the maximum velocities: 4.8, 4.3 and 3.6 m/s, for 0.97, 0.27 and 0.09 m/s^2, respectively. It is important to note that in order to keep the same notation used in the original experiments, we preserve the horizontal axis as free-stream velocity U, instead of u^*. Nevertheless, the transformation from one variable to the other is performed as in Ibrahim et al. (2003).

Using the KPR analysis stated in section 4, the maximum resuspension velocities as a function of the acceleration allow obtaining the value of the constant $A = \frac{1.61 a_0}{1.4\, R_p^2\, c_d \rho_f f r}$ which includes all the information related to the particle-surface system and air fluid parameters.

Thus, according to Eq. 18 we can plot the natural logarithm of $\frac{\alpha}{u_{max}^{*\,3}}$ as a function of $\frac{1}{u_{max}^{*\,2}}$.

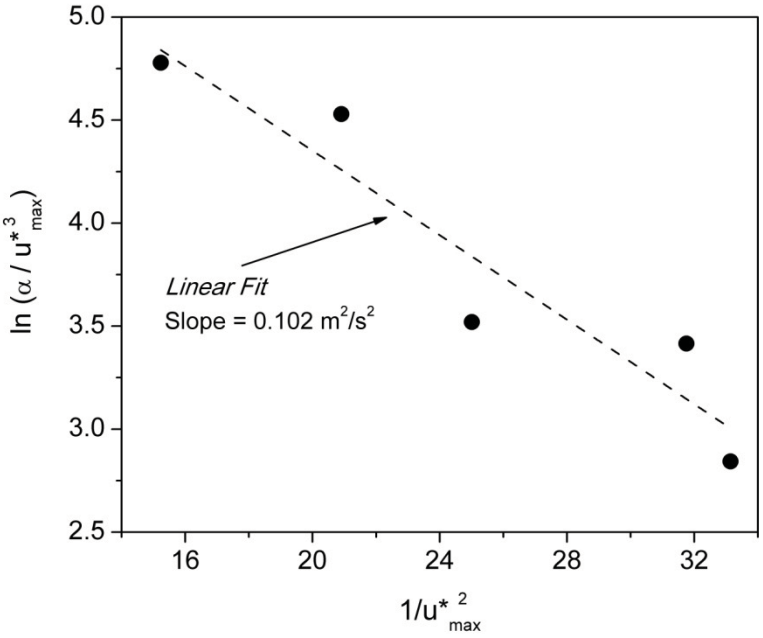

Figure 9: KPR application for the estimation of the unknown particle-surface constant *A* in experiments of Ibrahim et al. (2006).

As expected, we obtain the linear trend presented in Figure 9, whose slope *A* is 0.102 m^2/s^2.

In order to corroborate the prediction obtained by this KPR analysis, we perform MC simulations using the estimated value for *A*. We fix the values of the following parameters: particle radius R_p, air density ρ_f, contact radius a_0, and the constant c_d (Table 1). Thus, from *A*, we calculate the reduction factor f_r which takes into account the contact geometry in the real surface, giving a value of 52.

Monte Carlo results for the different accelerations are shown in Figure 10, along with the experimental data of Ibrahim et al. (2006). As it can be seen, the MC model predicts quite well the resuspended fraction as a function of the velocity U, especially for low accelerations values.

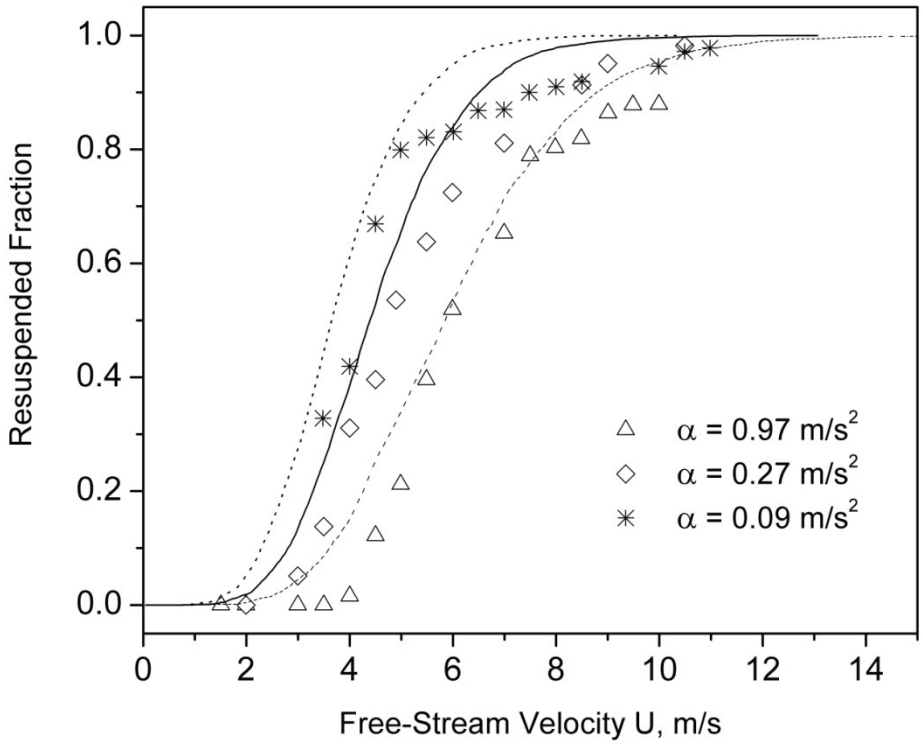

Figure 10: Comparison between experimental data (Ibrahim et al., 2006) and MC simulations for three different accelerations. Symbols represent the experimental results and lines the MC simulations.

It can be noted that, in general, the MC model overestimates the resuspended fraction. This could be related to the fact that in our MC model we do not include so far any change of the wall shear stress and burst-sweep events in the near-wall region with the acceleration (Ibrahim et al., 2006).

It is worth noting that, through the information obtained from the KPR technique, we are able to reproduce the experimental behavior only based on the variation of the drag force (and moment) with the velocity ramp. Thus, inside a given time interval, the increment in the drag force and its moment becomes larger for larger accelerations, resulting, as expected, in a faster kinetic process.

6. Summary and conclusions

The resuspension of particles from surfaces by air flow was studied under different accelerations using Monte Carlo simulations. Results show that air flow acceleration increase the velocity range needed for all the resuspension process. Nevertheless, this

process becomes faster when acceleration increases. To better understand this kinetic behavior related to the velocity ramp used, we developed a Kinetic Programmed Resuspension methodology, KPR, based on the analogy with the Temperature Programmed Desorption (TPD) technique.

This technique enables us to obtain, through simple calculations, a transcendental equation relating the friction velocity u^*_{max} with the air flow acceleration and other particle-substrate constants. As a consequence, the resuspension process kinetics is now characterized by analyzing the behavior of the particle flux as a function of the wind acceleration. Results demonstrate that the particle rate increases with acceleration. However, the air velocity at which one may expect the maximum flow rate results to be higher as acceleration increases.

The last part of this study was dedicated to corroborate the capability of the KPR technique to calculate particle-surface parameters typically unknown in an experimental scenario. This makes this technique a potential tool for the study of resuspension. This fact was demonstrated when comparing MC simulations (using the parameter obtained through KPR) with the experimental data.

Moreover, the technique presented here, provides a vision, from the physical foundations of statistical mechanics, which complements and broadens the understanding of the complex phenomenon of particle resuspension.

Future efforts would be devoted to better improve this technique with a particular focus on other possible applications and to include in our MC model the decrease of the burst-sweep events though a variation of the drag force dispersion with the acceleration.

References

Benito, J., Aracena, K. V., Uñac, R., Vidales, A., Ippolito, I., 2015. Monte Carlo modelling of particle resuspension on a flat surface. Journal of Aerosol Science 79, 126-139.

Benito, J., Uñac, R., Vidales, A., Ippolito, I., 2016. Validation of the Monte Carlo model for resuspension phenomena. Journal of Aerosol Science 100, 26-37.

Binder, K., Heermann, D., 1992. Monte Carlo simulation in statistical physics: An introduction. 2nd. ed. Berlin: Springer Verlag.

Bohme, G., Krupp, H., Rabenhorst, H., Sandstede, G., 1962. Adhesion measurements involving small particles. Transactions of the Institution of Chemical Engineers 40, 252-259.

Bowling, R., 1988. A theoretical review of particle adhesion, particles on surfaces i: Detection, adhesion and removal. New York: Plenum Press, 129-142.

Csavina, J., Field, J., M.P. Taylor, M., Gao, S., Landzuri, A., Betterton, E., Sez, A., 2012. A review on the importance of metals and metalloids in atmospheric dust and aerosol from mining operations. Science of the Total Environment 433, 58-73.

Falconer J. L., Schwarz J. A., 1983. Temperature- Programmed Desorption and Reaction: applications to Supported Catalysts, Catal. Rev.-Sci. Eng., 25(2), 141-227.

Fichthorn, K.A., Weinberg, W.H., 1991. Theoretical foundations of dynamical Monte Carlo simulations, J. Chem Phys. 95(2), 1090-1096.

Friess, H., Yadigaroglu, G., 2001. A generic model for the resuspension of multilayer aerosol deposits by turbulent flow. Nuclear Science and Engineering 138, 161-176.

Fu, S., Chao, C., SO, R., Leung, W., 2013. Particle resuspension in a wall bounded turbulent flow. Journal of Fluids Engineering 135, 041301.

Goldasteh, I., Goodarz, A., Ferro, A., 2013. Monte Carlo simulation of micron-size spherical particle removal and resuspension from substrate under fluid flows. Journal of Aerosol Science 66, 62-71.

Henry, C., Minier, J.-P., 2014a. Progress in particle resuspension from rough surfaces by turbulent flows. Progress in Energy and Combustion Science 45, 1-53.

Henry, C., Minier, J.-P., 2014b. A stochastic approach for the simulation of particle resuspension from rough substrates: Model and numerical implementation. Journal of Aerosol Science 77, 168-192.

Henry, C., Minier, J.-P., Lefreve, G., 2012. Numerical study on the adhesion and re-entrainment of non-deformable particles on surfaces: The role of surface roughness and electrostatic forces. Langmuir 28, 438-452.

Hughes, E. M., 1971. The chemical statics and kinetics of solutions. London: Academic Press.

Ibrahim, A., Dunn, P., Brach, R., 2003. Micro-particle detachment from surfaces exposed to turbulent air flow: controlled experiments and modeling. Journal of Aerosol Science 29, 765-782.

Ibrahim, A., Dunn, P., 2006. Effect of temporal flow on the detachment of micro-particles from surfaces. Journal of Aerosol Science 37, 1258-1266.

Ibrahim, A., Dunn, P., Qazi, M., 2008. Experiments and validation of a model for micro-particle detachment from a surface by turbulent air flow. Journal of Aerosol Science 29, 645-656.

Johnson, K., Kendall, K., Roberts, A., 1971. Surface energy and the contact of elastic solids. Proceedings of the Royal Society of London. Series A, Mathematical and Physical 324, 301-313.

Matsusaka, S., Aoyagi, T., Masuda, H., 1991. Unsteady particle re-entrainment model based on the internal adhesive strength distribution of a fine powder layer. Kagaku Kogaku Ronbunshu 17, 1194-1200.

Matsusaka, S., Masuda, H., 1996. Particle re-entrainment from a fine powder layer in a turbulent air flow. Aerosol Science and Technology 24, 69-84.

Mollinger, A. M., Nieuwstadt, F. T. M., 1996. Measurement of the lift force on a particle fixed to the wall in the viscous sub-layer of a fully developed turbulent boundary layer. Journal of Fluid Mechanics 316, 285-306.

Popovitch A. T. and Hummel R. L., 1967. Experimental Study of the Viscous Sub-layer in Turbulent Pipe Flow. AIChE Journal, 13, 854-860.

Redhead P. A., 1962. Thermal desorption of gases. Vacuum 12(4), 2013-211.

Reeks, M., Hall, D., 2001. Kinetic models for particle resuspension in turbulent flows: theory and measurement. Journal of Aerosol Science 32, 1-32.

Reeks, M., Reed, J., Hall, D., 1988. On the resuspension of small particles by a turbulent flow. Journal of Physics D: Applied Physics 21, 574-598.

Salazar-Banda, G., Felicetti, M., Gonalves, J., Coury, J., Aguiar, M., 2007.Determination of the adhesion force between particles and a flat surface, using the centrifuge technique. Powder Technology 173, 107-117.

Sales, J., Uñac, R., Gargiulo, M., Bustos, V., Zgrablich, G., 1996. Monte Carlo simulation of temperature programmed desorption spectra: A guide through the forest for monomolecular adsorption on a square lattice. Langmuir 12, 95-100.

Soltani M., Ahmadi G., 2006. Particle Removal Mechanism under substrate acceleration. The Journal of adhesion 44:3, 161-175.

Spinicci R., 1997. A method for simulating temperature programmed desorption peaks. Thermochimica Acta 296, 111-121.

Stempniewicz, M., Komen, E., de With, A., 2008. Model of particle resuspension in turbulent flows. Nuclear Engineering and Design 238, 2943-2959.

Stovern, M., Felix, O., Csavina, J., Rine, K., Russell, M. R., Jones, R., King,M., Betterton, E., Sez, A., 2014. Simulation of windblown dust transport from a mine tailings impoundment using a computational fluid dynamics model. Aeolian Research 14, 75-83.

Taheri, M., Bragg, G., 1992. A study of particle resuspension in a turbulent flow using a preston tube. Aerosol Science and Technology 16, 15-20.

Wang G.-W., (1983).Temperature-programmed Desorption Study of Carbon Monoxide Adsorbed on Magnesium Oxide J. *Chem.* SOC., Faraday Trans 79, 1373-1380.

Wen, H., Kasper, G., 1989. On the kinetics of particle re-entrainment from surfaces. Journal of Aerosol Science 20, 483-498.

Zhang, F., 2011. The modelling of particle resuspension in a turbulent boundary layer. Ph.D. thesis, School of Mechanical and System Engineering Newcastle University, United Kingdom, and Laboratoire de Mecanique des Fluides et d' Acoustique Ecole Centrale de Lyon, France, and references there in.

Zhang, F., Reeks, M., Kissane, M., 2013. Particle resuspension in turbulent boundary layers and the influence of non-gaussian removal forces. Journal of Aerosol Science 58, 103-128.

Ziskind, G., Fichman, M., Gutfinger, C., 1995. Resuspension of particles from surfaces to turbulent flows - review and analysis. Journal of Aerosol Science26, 613-644.

Figure Captions

Figure 1: Particle Force diagram.

Figure 2: MC model results of Resuspended Fraction vs. Friction velocity u^* for three different accelerations. Dash-dotted horizontal line corresponds to a resuspended fraction of 0.5, from which the threshold velocity u_{th}^* was evaluated.

Figure 3: MC model results for Resuspended Fraction vs. Time corresponding to three different accelerations.

Figure 4: Particle Flux vs. Friction velocity u^* using our MC model, for three different accelerations. Vertical arrows indicate maximum's locations.

Figure 5: Dependence of the u_{max}^* as a function of the air flow acceleration. Symbols represent the maximum velocities obtained through our MC curves for different accelerations. Solid line represent the KPR prediction from Eq. 17.

Figure 6: Illustration of the KPR application for the estimation of the unknown particle-surface constant *A*.

Figure 7: Particle Flux vs. Time for three different accelerations obtained from our MC model results.

Figure 8: Particle Flux vs. Free-Stream Velocity U for three different accelerations, obtained from the experimental data analysis of Ibrahim et al. (2006). Vertical axis represents the Flux divided the initial amount of particles.

Figure 9: KPR application for the estimation of the unknown particle-surface constant *A* in experiments of Ibrahim et al. (2006).

Figure 10: Comparison between experimental data (Ibrahim et al., 2006) and MC simulations for three different accelerations. Symbols represent the experimental results and lines the MC simulations.

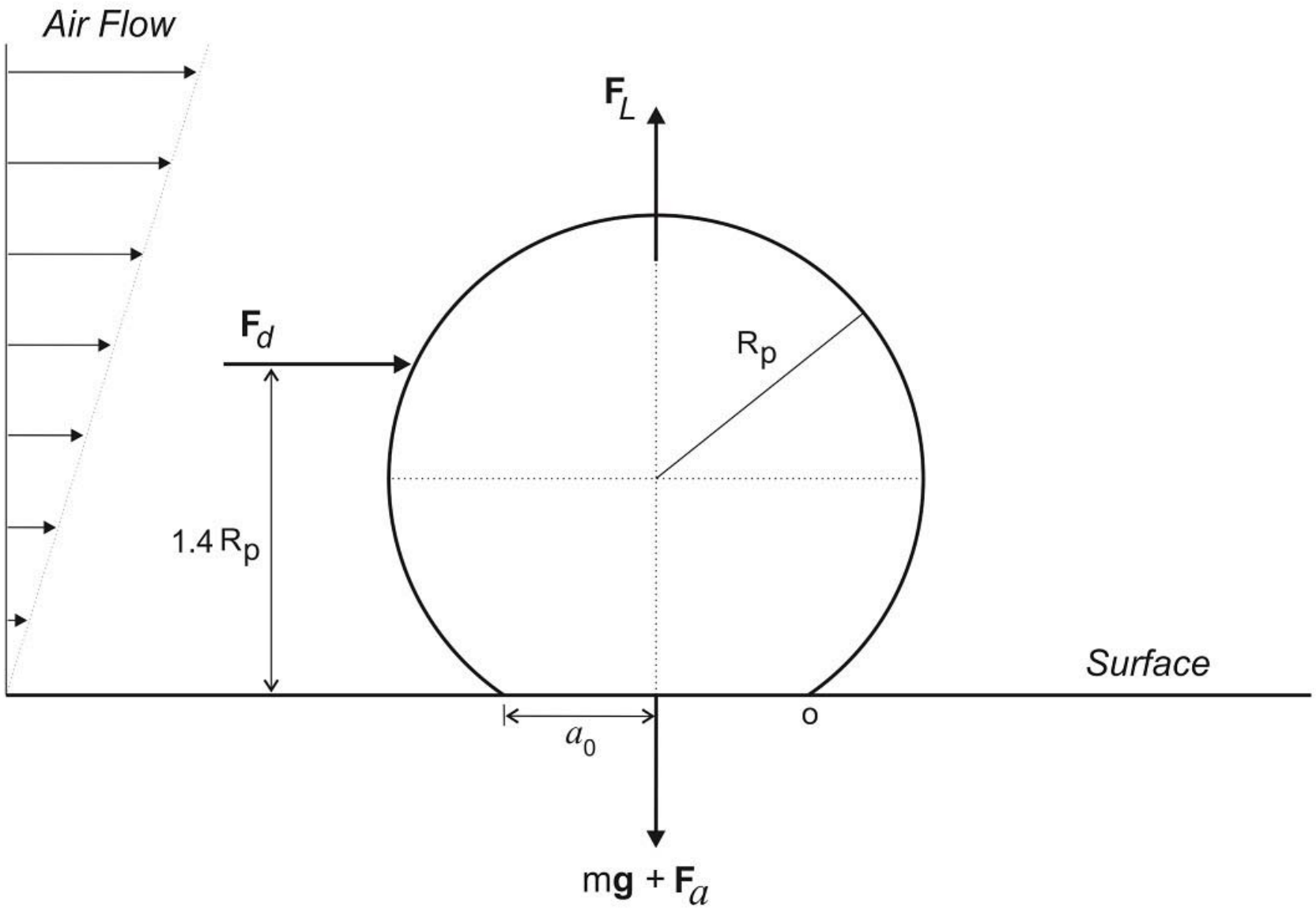
Air Flow
$\mathbf{F}_L$
$\mathbf{F}_d$
R_p
$1.4\,R_p$
Surface
a_0
o
$m\mathbf{g} + \mathbf{F}_a$

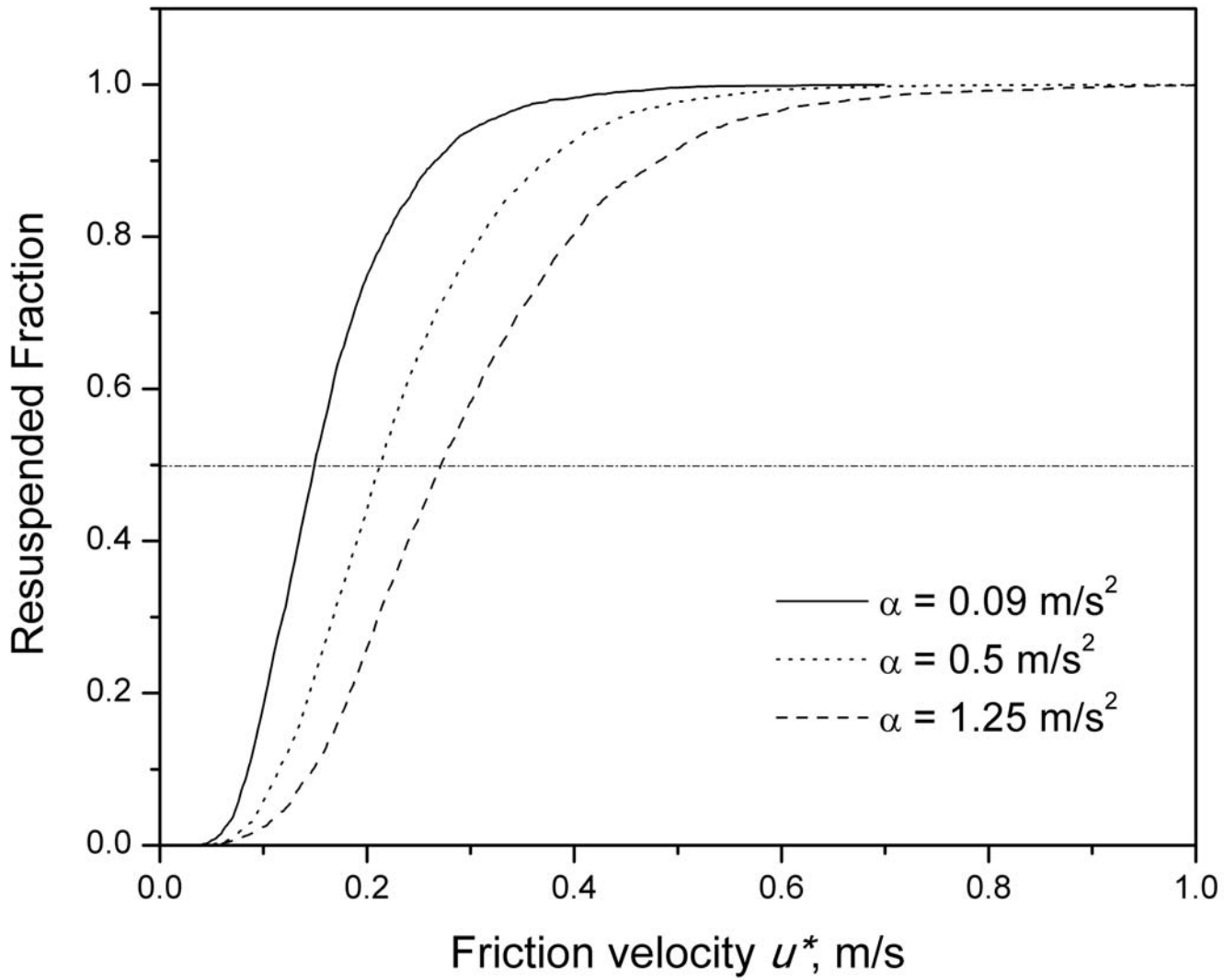
Resuspended Fraction
1.0
0.8
0.6
0.4
0.2
0.0
0.0
0.2
0.4
0.6
0.8
1.0
Friction velocity u*, m/s
α = 0.09 m/s²
α = 0.5 m/s²
α = 1.25 m/s²

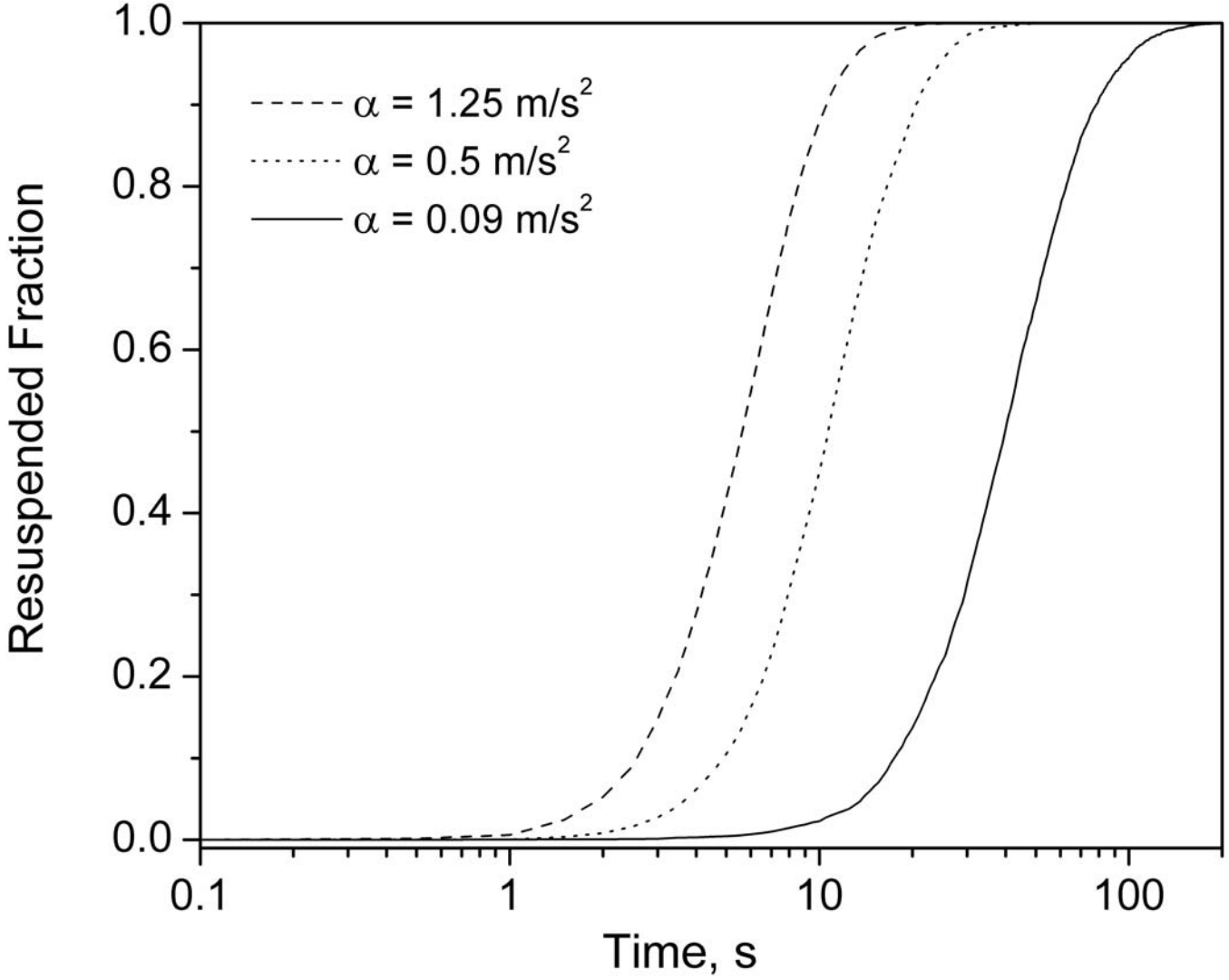
Resuspended Fraction
1.0
0.8
0.6
0.4
0.2
0.0
0.1
1
10
100
Time, s
α = 1.25 m/s²
α = 0.5 m/s²
α = 0.09 m/s²

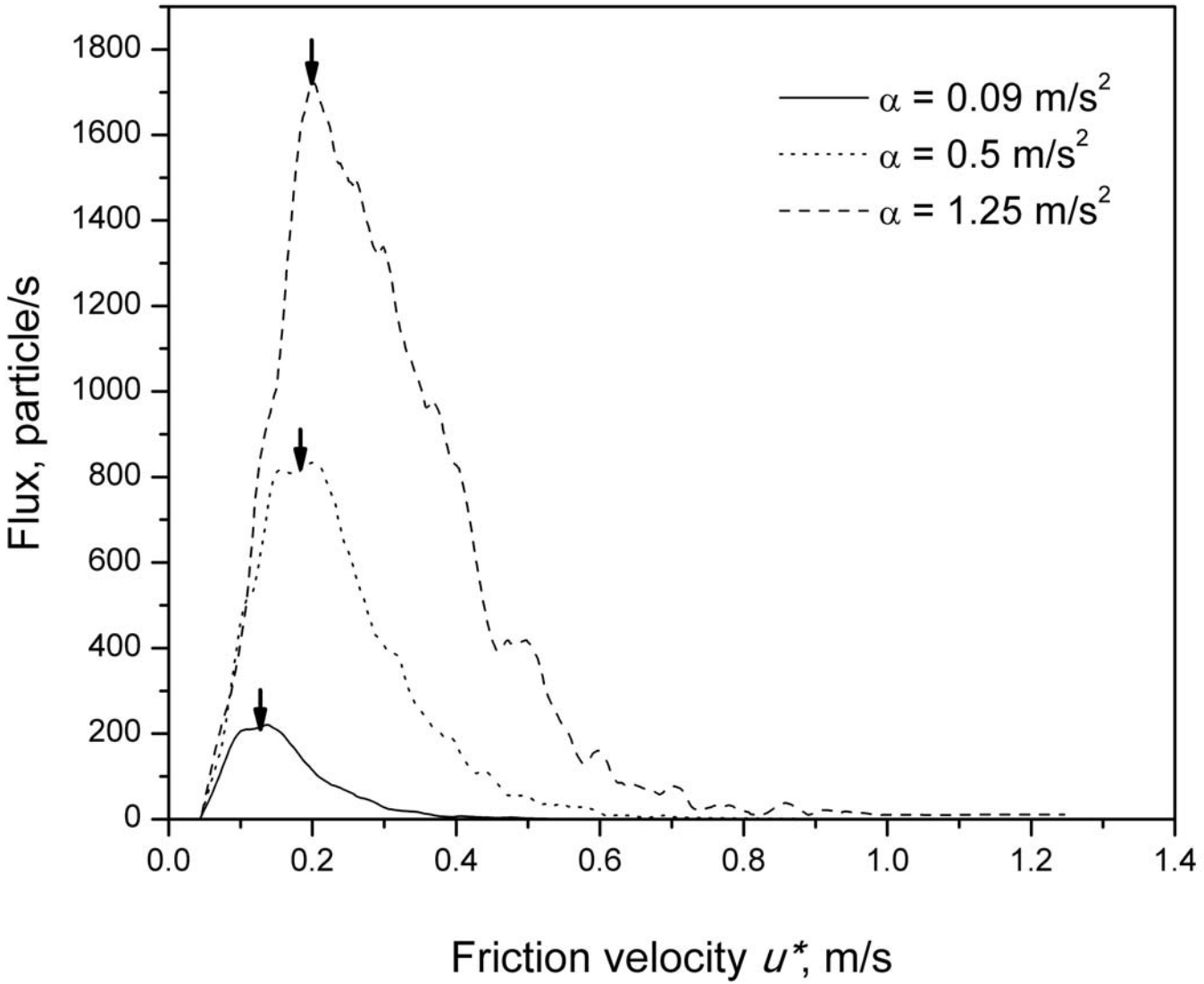
Flux, particle/s
1800
1600
1400
1200
1000
800
600
400
200
0
0.0
0.2
0.4
0.6
0.8
1.0
1.2
1.4
Friction velocity u*, m/s
α = 0.09 m/s²
α = 0.5 m/s²
α = 1.25 m/s²

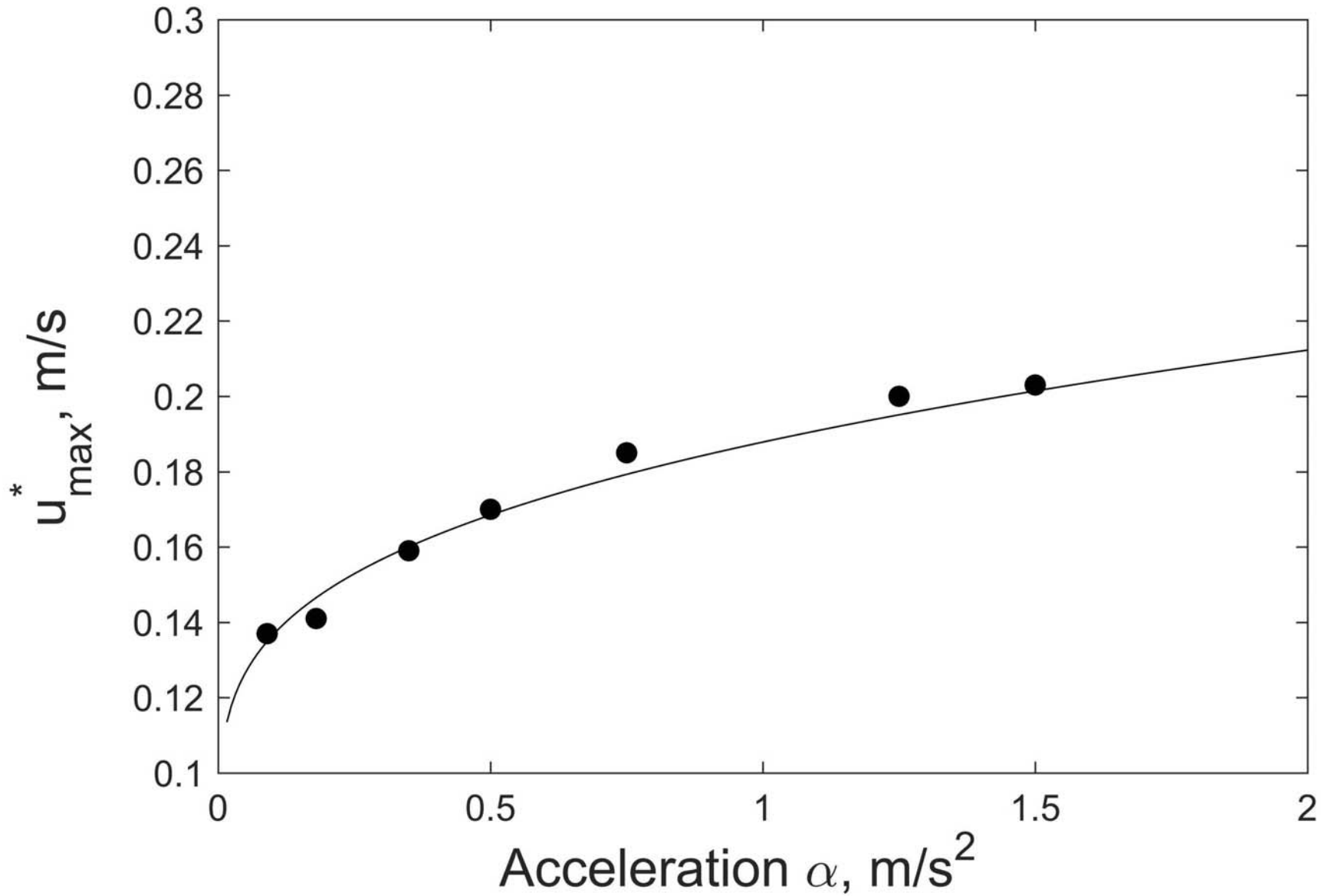
0.3
0.28
0.26
0.24
0.22
0.2
0.18
0.16
0.14
0.12
0.1
u^*_{max}, m/s
0
0.5
1
1.5
2
Acceleration α, m/s^2

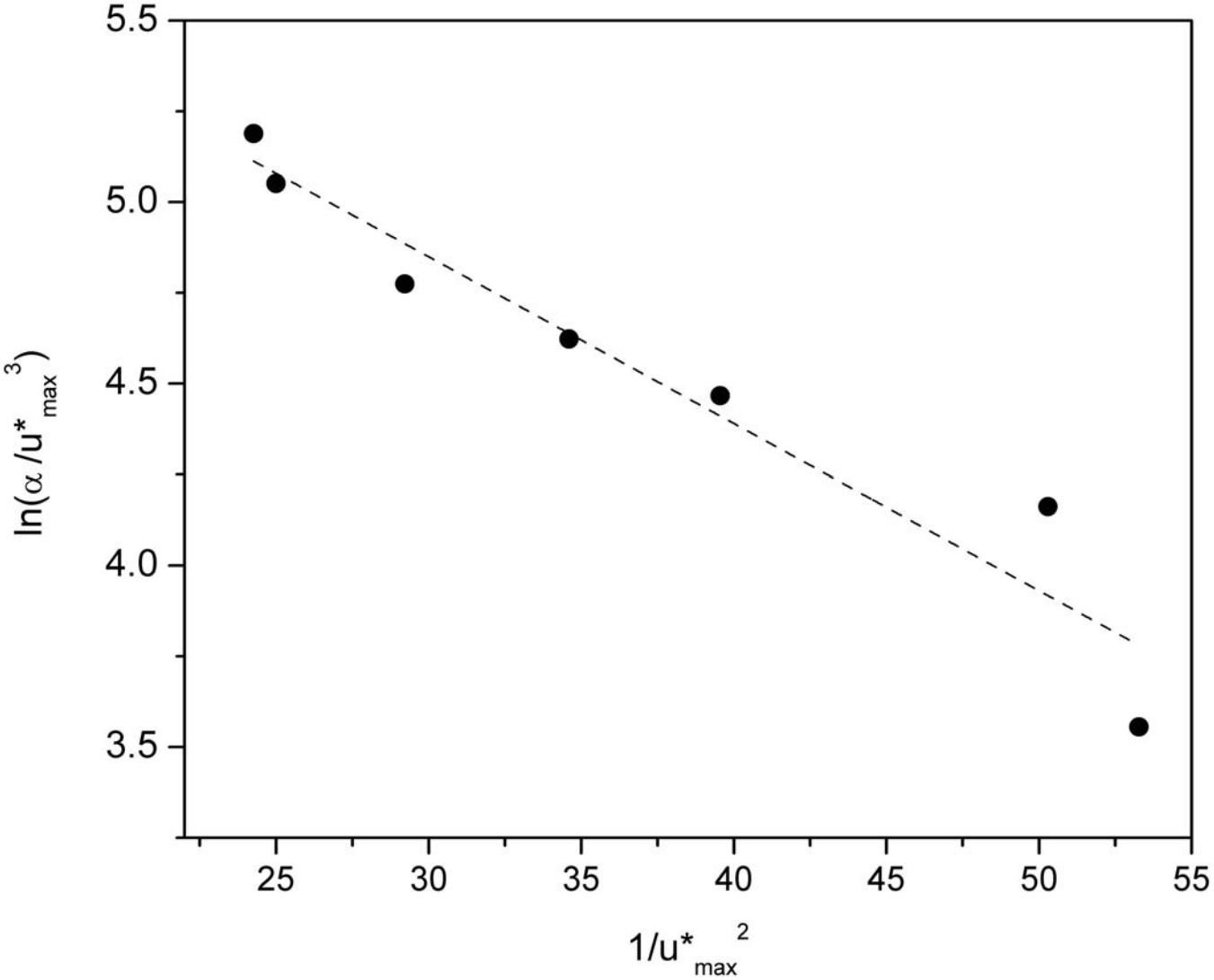
5.5
5.0
4.5
4.0
3.5
ln(α /u*max3)
25
30
35
40
45
50
55
1/u*max2

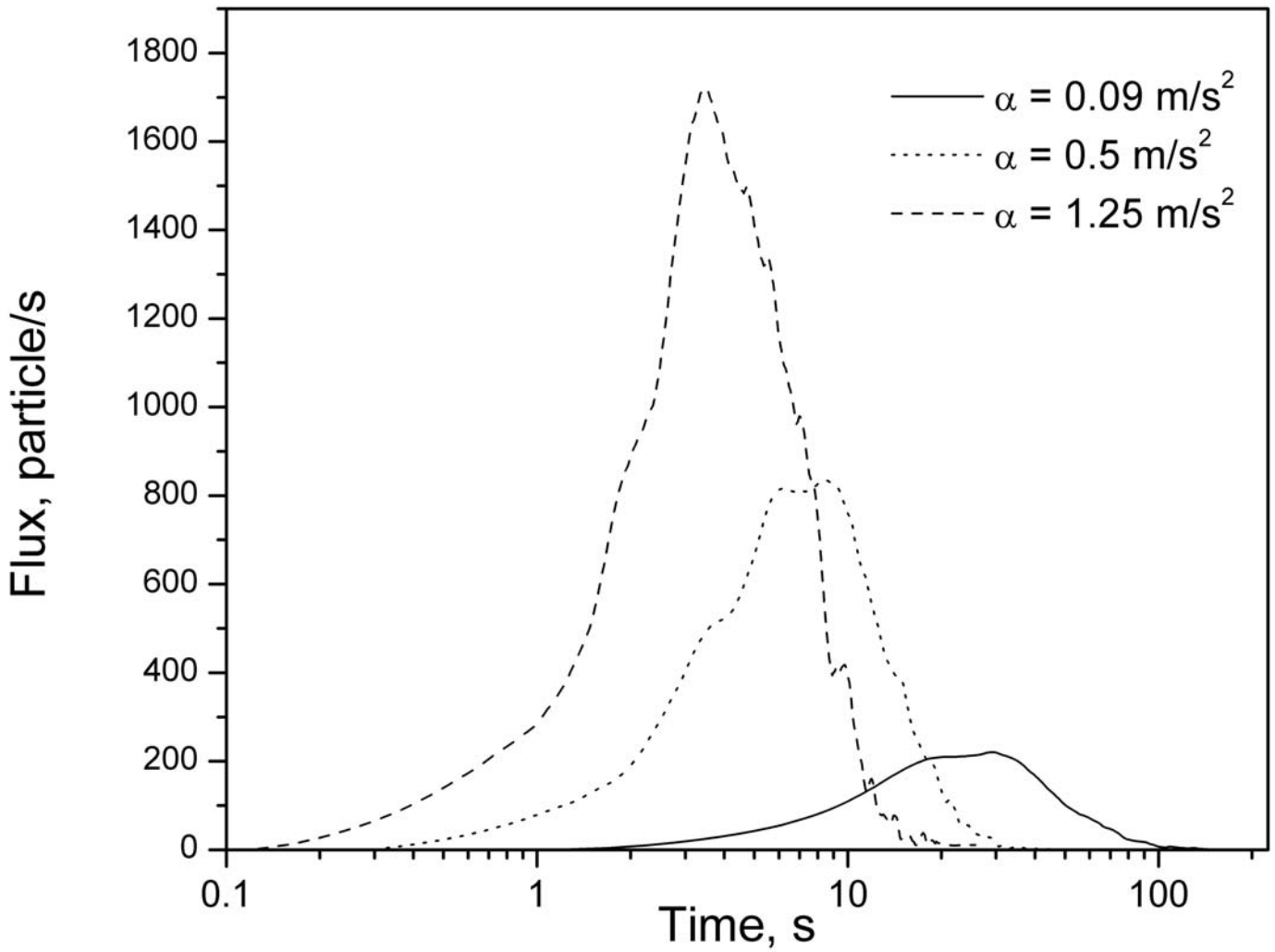
Flux, particle/s
Time, s
α = 0.09 m/s²
α = 0.5 m/s²
α = 1.25 m/s²
0
200
400
600
800
1000
1200
1400
1600
1800
0.1
1
10
100

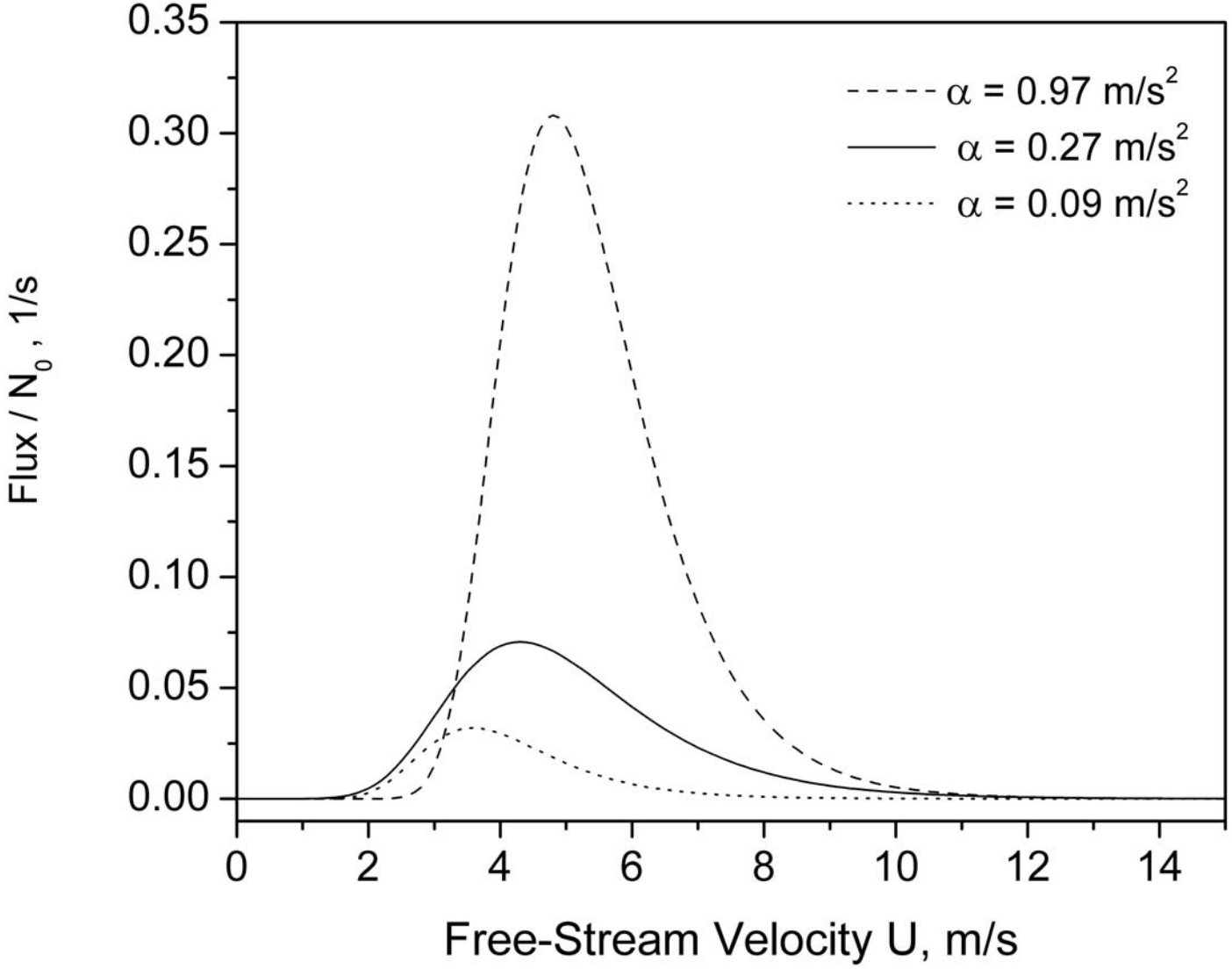
0.35
0.30
0.25
0.20
0.15
0.10
0.05
0.00
Flux / N0 , 1/s
α = 0.97 m/s2
α = 0.27 m/s2
α = 0.09 m/s2
0
2
4
6
8
10
12
14
Free-Stream Velocity U, m/s

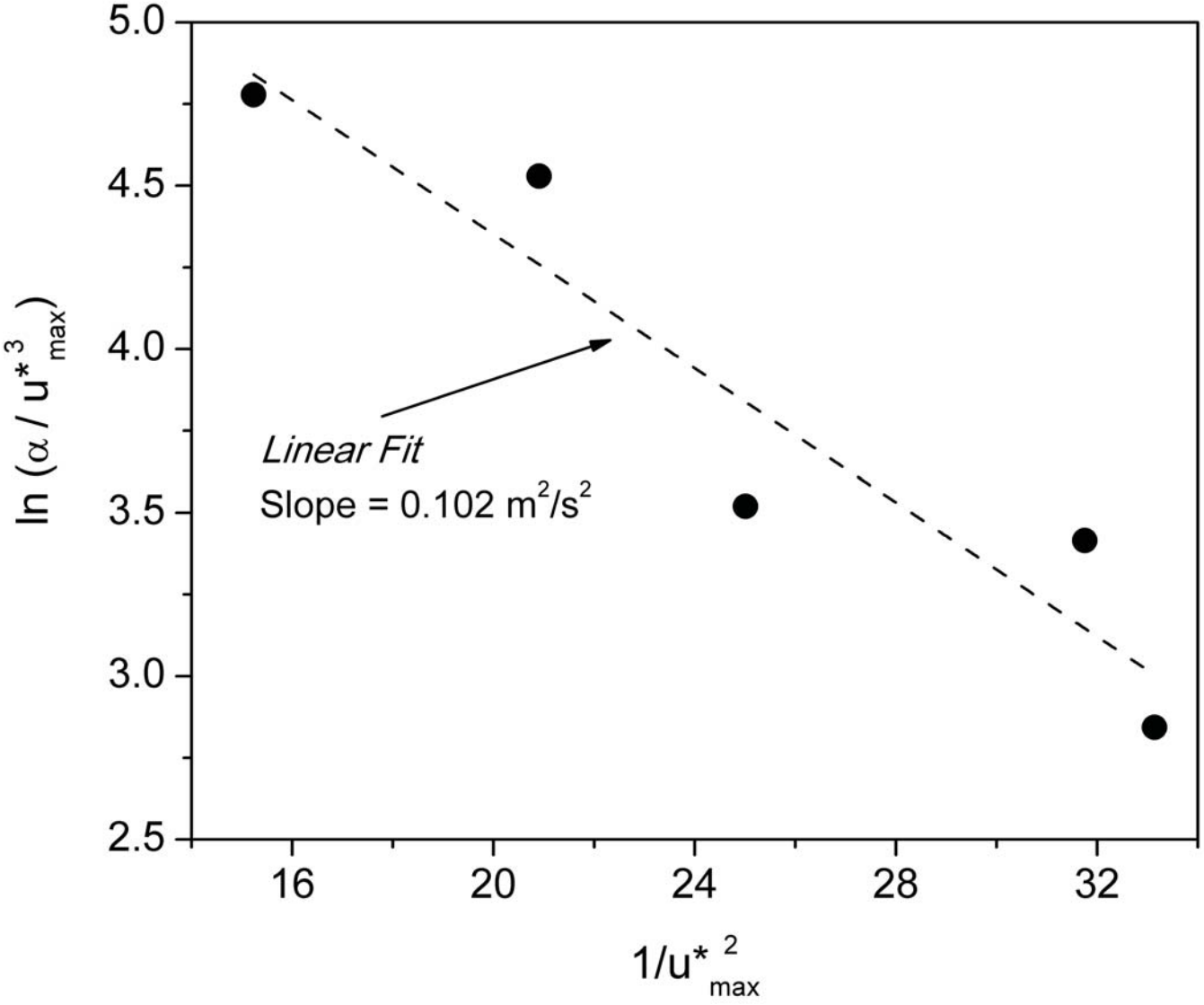
5.0
4.5
4.0
3.5
3.0
2.5
16
20
24
28
32
ln (α / u*3max)
1/u*2max
Linear Fit
Slope = 0.102 m2/s2

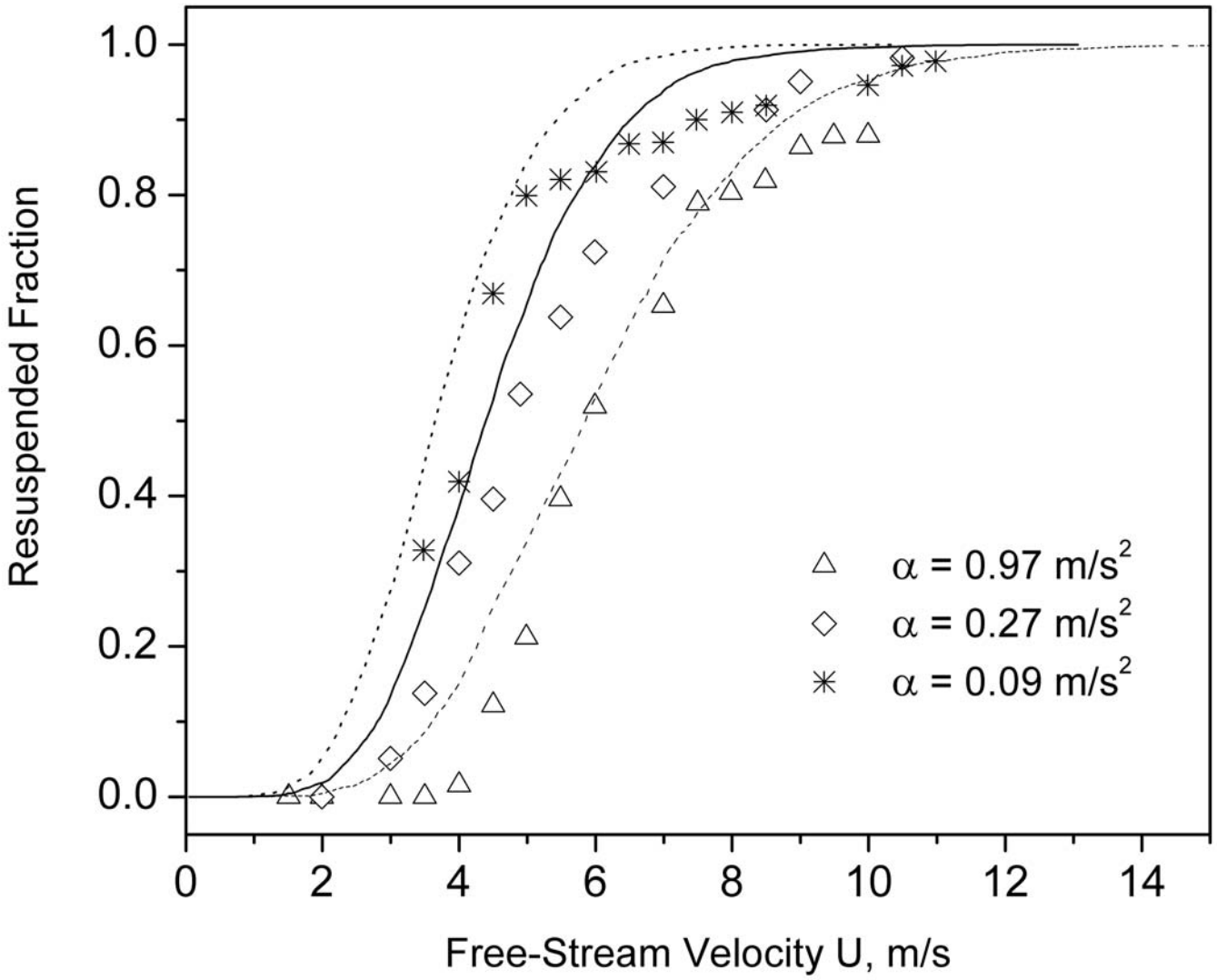
Resuspended Fraction
1.0
0.8
0.6
0.4
0.2
0.0
0
2
4
6
8
10
12
14
Free-Stream Velocity U, m/s
α = 0.97 m/s²
α = 0.27 m/s²
α = 0.09 m/s²

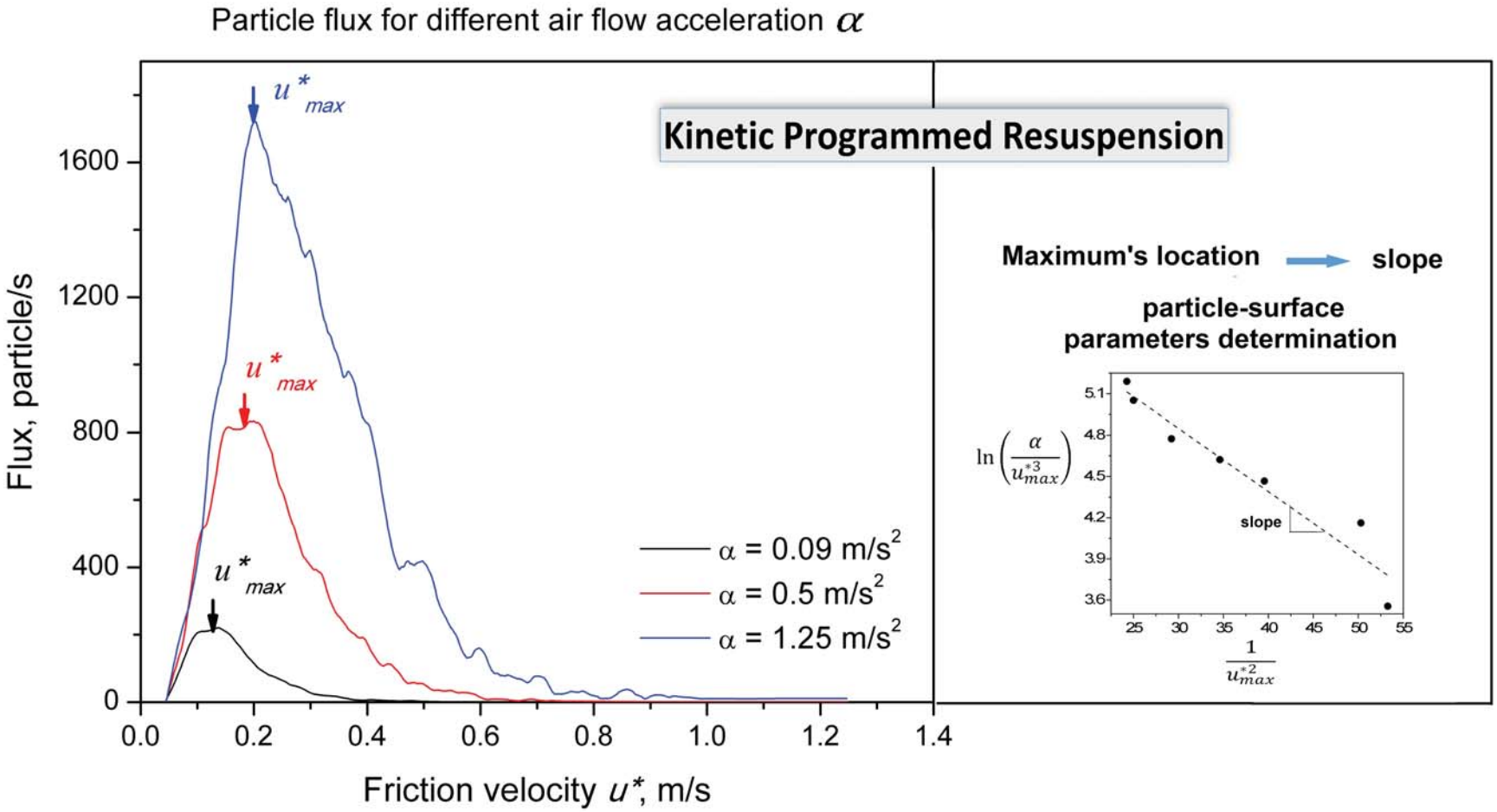
Particle flux for different air flow acceleration α
Kinetic Programmed Resuspension
u^*_{max}
u^*_{max}
u^*_{max}
α = 0.09 m/s²
α = 0.5 m/s²
α = 1.25 m/s²
Flux, particle/s
Friction velocity u^*, m/s
0
400
800
1200
1600
0.0
0.2
0.4
0.6
0.8
1.0
1.2
1.4
Maximum's location → slope
particle-surface parameters determination
$\ln\left(\frac{\alpha}{u^{*3}_{max}}\right)$
$\frac{1}{u^{*2}_{max}}$
slope
5.1
4.8
4.5
4.2
3.9
3.6
25
30
35
40
45
50
55

Table 1: Simulation constants and particle-surface parameters.

JKR Adhesion force (N)	$1.61R_p$
Reduction Factor f_r	100 and 52
Adhesion dispersion σ_a	1.0
Surface energy γ (J/m^2)	0.15
Surface Young's modulus E_1 (GPa)	80.1
Surface Poisson's ratio ν_1	0.27
Particle Young's modulus E_2 (GPa)	215
Particle Poisson's ratio ν_2	0.28
Particle Density ρ (Kgm^{-3})	8000
Air Density ρ_f (Kgm^{-3})	1.2
Air kinetic viscosity ν (m^2/s)	1.45E-5
Drag force constant c_d	32.0
Frequency k (1/s)	1.0